Journal of Materials Chemistry C

Anion Chemical Composition of Poly(ethylene oxide)-based Sulfonylimide and Sulfonate Lithium Ionomers Controls Ion Aggregation and Conduction

Journal:	*Journal of Materials Chemistry C*
Manuscript ID	TC-ART-05-2022-002212.R1
Article Type:	Paper
Date Submitted by the Author:	07-Aug-2022
Complete List of Authors:	Colby, Ralph; Penn State, Materials Science and Engineering Hickey, Robert; Pennsylvania State University, Materials Science and Engineering Madsen, Louis; Virginia Tech, Chemistry Mei, Wenwen ; Penn State University Park, MATSE Yu, Deyang; Virginia Polytechnic Institute and State University, Macromolecules Innovation Institue and Department of Chemistry George, Christy; Penn State - Main Campus

Anion Chemical Composition of Poly(ethylene oxide)-based Sulfonylimide and Sulfonate Lithium Ionomers Controls Ion Aggregation and Conduction

Wenwen Mei[1], Deyang Yu[2], Christy George[3], Louis A. Madsen[2], Robert J. Hickey[1,4,*], Ralph H. Colby[1,4,*]

[1]Materials Science and Engineering, The Penn State University, University Park, PA16802, USA

[2]Department of Chemistry and Macromolecules Innovation Institute, Virginia Tech, Blacksburg, VA 24061

[3]Department of Chemistry, The Penn State University, University Park, PA16802, USA

[4]Materials Research Institute, The Penn State University, University Park, PA16802, USA

*Corresponding Authors: rjh64@psu.edu and rhc5@psu.edu

Abstract

Maximizing ion conduction in single-ion-conducting ionomers is essential for their application in energy-related technologies such as Li-ion batteries. Understanding the anion chemical composition impacts on ion conduction offers new perspectives to maximize ion transport, since the current approach of lowering T_g has apparently reached a limit (lowest T_g ~ 190 K, highest conductivity ~ 10^{-5}–10^{-4} S/cm). Here, a series of random ionomers are synthesized by copolymerizing poly(ethylene glycol) methacrylate with either sulfonylimide lithium methacrylate (MTLi) or sulfonate lithium methacrylate (MSLi) using reversible addition-fragmentation chain transfer (RAFT) polymerization. Li-ion conduction and self-diffusion coefficients (D_{Li+}) of the ionomers are characterized with dielectric relaxation spectroscopy (DRS) and pulsed-field-gradient (PFG) NMR diffusometry, respectively. Increasing ion content decreases the Li-ion conductivity and D_{Li+}, as expected from the increased T_g. Moreover, a considerably lower ionic conductivity and D_{Li+} are observed for MSLi compared to MTLi at constant ion content and T_g/T. As revealed from X-ray scattering, strong ion aggregation in MSLi results in much lower conductivity and D_{Li+} compared with less aggregated MTLi based on the more delocalized sulfonylimide anion. These results emphasize the detrimental and molecularly specific role of ion

aggregation on Li-ion conductivity, and highlight the necessity for minimizing ion aggregation via the rational choice of anion chemical composition.

Introduction

Polymer materials are desirable and versatile components that enable technology advances in energy-related applications such as flexible electronics,[1-4] lightweight solar cells,[5-8] and safe batteries.[9-13] There are inherent advantages of polymers over different classes of materials with respect to mechanical integrity, easy processing, low cost, and tailorable properties based on polymer composition, that drive widespread implementation in current commercial products.[5, 11, 12, 14, 15] For example, it is envisioned that polymer electrolytes will mitigate the safety issue related to flammable liquid electrolytes, lead to long-term stability due to reduced volume changes during charge/discharge processes, and enable the development of high-energy-density batteries using lithium metal electrodes.[9-13, 16] The success of polymer electrolytes will also advance the development of solid-state batteries for grid-scale energy storage.[11, 15, 17] Polymer material improvements have considerable implications for addressing grand societal challenges related to energy storage and transitioning to sustainable and renewable energies.[9-11, 13, 15] Although the benefits of single-ion conducting polymer electrolytes are tremendous, ionic conductivity is still below the necessary threshold for many commercial applications.

There are two main types of polymer electrolytes: single-ion conducting ionomers and dual-ion conductors.[18, 19] Single ion-conducting polymers in which the Li-ion is the mobile cation exhibit high transference numbers due to the anion being attached to the polymer backbone.[16, 19-21] Dual-ion polymer electrolytes typically contain a mixture of a neutral polymer such as poly(ethylene oxide) (PEO) and salt (e.g., bis(trifluoromethane)sulfonylimide lithium salt (LiTFSI)), where cations and anions both contribute to the conductivity.[18] High transference number (~ 1) is expected to prevent Li dendrite formation by reducing concentration polarizations of anions that is detrimental to cell performance.[16, 20-26] However, unplasticized single-ion conducting ionomers show low conductivity at ambient temperature, which is orders of magnitude lower than the desired conductivity of 10^{-3} S/cm for device operation.[16, 27-29] Maximizing ion transport remains the critical challenge for the practical applications of single ion-conducting polymers.

Understanding how the chemical composition of single-ion conducting ionomers affects ion conduction is essential to promote ionic conductivity and enable the rational design of polymers with optimal compositions and structures. The emerging single-ion conducting ionomers with bulky ions (e.g., $TFSI^-$, $PF6^-$) show significantly higher conductivity than the conventional

polyelectrolytes. However, such a conductivity improvement is not well understood, and the discussions for the conductivity difference from different polymer structures focus primarily on the effects of glass transition temperature (T_g).[29-39] A closer look at literature data comparing the conductivity at reduced temperature T_g/T suggests T_g is not the exclusive factor that dictates conductivity.[29, 34-41] For example, there are discrepancies between conductivities for ionomers with different ion chemical compositions. Specifically, homopolymer poly(imidazolium methacrylate) with PF_6^- counterion demonstrate an order of magnitude higher conductivity than that with $TFSI^-$ counterion at the same T_g/T.[37] Similarly, with the same counterion and at the same T_g/T, phosphonium polymerized ionic liquids demonstrate orders of magnitude higher conductivity than ammonium polymerized ionic liquids.[36, 38] For block copolymers with poly(imidazolium) mid-block, more than an order of magnitude higher conductivity is observed with Br^- counterion compared with $TFSI^-$ counterion at the same T_g/T.[40] Such an ion chemical composition dependence for conductivity offers new perspectives on the design of highly conductive ionomers, if the impacts of ion composition on ion conduction can be fully understood, since the current efforts in lowering polymer T_g to promote conductivity have in many ways reached a limit.[16, 20, 21, 42-46] To the authors' knowledge, the minimum T_g achieved have been 203 K for Li^+ conducting single-ion

conductors and 187 K for Br^- conducting single-ion conductors and the largest ionic conductivities achieved at room temperature have been ~ 10^{-5}–10^{-4} S/cm.[21, 31, 47-50]

Understanding the impacts of anion chemical composition and structure on Li^+ conduction in ionomers will guide polymer electrolyte design with the goal of maximizing ion transport. To this end, here, Li-ion conduction in two random copolymers containing prototypical anion chemical compositions are reported: sulfonylimide and sulfonate. A series of random copolymers with different ion contents were synthesized by copolymerizing either sulfonylimide lithium methacrylate or sulfonate lithium methacrylate with poly(ethylene glycol) methacrylate (PEO9) using reversible addition-fragmentation chain transfer (RAFT) polymerization. Random copolymers MTLi (sulfonylimide) and MSLi (sulfonate) exhibit similar molecular weight and narrow dispersity. The conductivity and Li-ion mobility were measured using dielectric relaxation spectroscopy (DRS) and pulsed-field-gradient (PFG) NMR diffusometry, demonstrating more than an order of magnitude higher conductivity and Li^+ diffusivity despite a higher T_g for MTLi than MSLi at equivalent ion content (i.e., MSLi19 and MTLi20). X-ray scattering reveals that the low conductivity of MSLi arises from significant ion aggregation, where aggregates are seen for

samples with ion content as low as 0.19 mol fraction (molar ratio of Li^+/EO = 0.027, **Table 1**) and is enhanced with increasing ion content. In contrast, ion pairs are better solvated by the PEO matrix for MTLi, resulting in much higher conductivity and Li^+ diffusivity. This work highlights the significant impacts of polymer-fixed anion chemical composition on the ionomer morphology and consequently ion conduction and emphasizes the need to reduce ion aggregation when designing polymeric ion conductors.

Experimental

Materials

2,2′-Azobis(2-methylpropionitrile) (98%), 4-cyano-4-(phenylcarbonothioylthio)pentanoic acid (> 97%), *N*, *N*-dimethylformamide (anhydrous, 99.8%), 3-sulfopropyl methacrylate potassium (98%), and lithium chloride (99%) were purchased from Sigma-Aldrich and used as received. Tetrahydrofuran (THF), acetone, and methanol (MeOH) were purchased from Fisher Scientific and used as received. Poly(ethylene glycol) methacrylate (average M_n = 500 g/mol) (PEO9) was purchased from Sigma-Aldrich and passed through neutral aluminum oxide (activated) before use. Lithium 3-[(trifluoromethane)sulfonamidosulfonyl]propyl methacrylate was purchased from Specific Polymers and used as received. Deuterated water (D_2O) for ^1H NMR spectroscopy was purchased from Sigma-Aldrich.

Synthesis of Single Ion Conducting Ionomers

Single ion-conducting ionomers were synthesized using reversible addition-fragmentation chain transfer (RAFT) polymerization of PEO9 and either lithium 3-[(trifluoromethane)sulfonamidosulfonyl)propyl methacrylate (MTLi) or 3-sulfopropyl methacrylate potassium (MSK) with 4-cyano-4-(phenylcarbonothioylthio)pentanoic acid as the RAFT agent, resulting in poly(MTLi-*co*-PEO9) and poly(MSK-*co*-PEO9) (**Figure 1**). A typical procedure for the synthesis of poly(MSK-*co*-PEO9) was as follows: 11.4 g PEO9, 1.3 g MSK, 54.1 mg 4-cyano-4-(phenylcarbonothioylthio)pentanoic acid, and 4.4 mg 2,2′-Azobis(2-methylpropionitrile) were dissolved in 20 mL DMF/water solution (10 vol% water). The solution was then degassed with Ar for 50 min. After degassing, the solution was stirred under Ar at 68 °C for 8 h. The polymerization was quenched in an ice bath and then exposed to air. The solution was transferred to a dialysis bag and dialyzed against 5 portions, each with a 100x excess of methanol over five days to remove unreacted monomers. Then 50 molar excess of LiCl compared to $SO_3^-K^+$ was added to the solution and stirred for one week. The excess LiCl was removed by dialyzing the polymer solution against 5 portions, each with a 100x excess of methanol for one week until the dialyzate reached the conductivity of the pure methanol (~0.08 μS/cm). The polymer solution was condensed with a rotatory evaporator and dried in the vacuum oven at 60 °C for 72 h. The synthesized copolymers are stored in a glovebox under dry argon before other characterizations.

Polymer Characterization

Size Exclusion Chromatography: The number-average PEG-equivalent molecular weight (M_n) and dispersity ($Đ$) of synthesized ionomers were measured using size exclusion chromatography (SEC) (Waters Corporation) with two Styragel HR columns (HR4-HR2) and a refractive index detector (Waters 2414). 0.5 M LiBr/DMF was used as the mobile phase with a 0.35 ml/min flow rate at 40

°C. Molecular weight calibration was performed with poly(ethylene glycol) standards (Fluka). The SEC results are listed in **Table 1,** and the SEC traces are shown in the Supporting Information **Figure S1**.

Nuclear Magnetic Resonance Spectroscopy: The composition of the synthesized copolymers was determined from ^{1}H NMR (Bruker NEO-400) in D_2O. Details of the determination of copolymer composition and typical ^{1}H NMR spectra are shown in the Supporting Information (**Figure S2** and **Figure S3**). The determined copolymer composition is very close to the monomer feed composition shown in **Figure S4a**, suggesting the synthesized ionomers are random copolymers with similar reactivity ratios (**Figure S4b**). The M_n determined from end group analysis are listed in **Table 1**.

Thermal Characterization

Thermal properties of synthesized ionomers were characterized with TA Q2000 differential scanning calorimeter (DSC). All the synthesized random copolymers are amorphous, and no crystallization or melting peaks are observed in the temperature range of -80 to 150 °C. The glass transition temperature (T_g) is taken as the midpoint of the heat capacity change in the second heating (20 K/min for heating and prior cooling) and listed in **Table 1**.

Table 1. Characterization results of synthesized single-ion conducting ionomers.

Sample[a]	M_n ($Đ$)[b], g/mol	M_n[c], g/mol	T_g[d], K	Li$^+$/EO	n_0[e], nm^{-3}

MTLi20	44,500 (1.33)	68,970	223	0.027	0.29
MTLi37	48,200 (1.31)	61,500	244	0.067	0.58
MTLi52	45,800 (1.25)	63,100	271	0.125	0.88
MSLi19	41,600 (1.23)	49,300	218	0.026	0.29
MSLi37	33,500 (1.19)	53,300	225	0.067	0.65
MSLi48	32,500 (1.17)	54,400	229	0.10	0.92

a. Numbers on the right of the polymer abbreviation denote the ion content (mol%) in the random copolymer (e.g., the ion content for MTLi20 is 20 mol%).

b. Measured with SEC in 0.05 M LiBr/DMF based on poly(ethylene glycol) standards.

c. Determined with end-group analysis from ^{1}H NMR (see SI for details)

d. Measured with DSC with 20 K/min heating and cooling rates.

e. The number density of cation and anion based on mass density ρ = 1.3 g/ml.

Dielectric Relaxation Spectroscopy (DRS)

DRS measurements were carried out using a Novocontrol GmbH concept 40 broadband dielectric spectrometer in the frequency range of 10^{-1}–10^7 Hz under 0.05 V (AC). Temperature control was achieved by using a Quatro N_2 cryostat. All measurements were performed with the standard parallel plate sample cell using 10 mm (top) and 30 mm (bottom) stainless steel electrodes. Sample

thickness was controlled by silica spacers with 100 μm thickness. The thickness of the measured samples was checked with a micrometer after measurement. After sandwiching the sample between electrodes with spacer, each sample was first dried in the vacuum oven at 60 °C for 48 h and further annealed in the Novocontrol spectrometer at 120 °C for 45 min to remove any moisture acquired during sample loading. Data were collected in isothermal frequency sweeps from 120 °C to -80 °C.

Small- and Wide- Angle X-ray scattering (SAXS/WAXS)

Samples were prepared by dissolving dry ionomer samples in methanol to form a viscous polymer solution. The polymer solutions were loaded into 1.5 mm diameter quartz capillaries (Charles Supper Company) and first dried under vacuum at 40 °C for 48 h and then at 80 °C for 72 h to remove methanol and water. Samples were annealed at 120 °C overnight before sealing the capillary with epoxy. Synchrotron X-ray scattering experiments were conducted at the 11-BM CMS beamline of the National Synchrotron Light Source II (NSLS-II) at Brookhaven National Laboratory. The beamline utilized X-rays with an energy of ~13.5 keV and a beam size of 0.02 x 0.05 mm^2. Two area detectors, Pilatus2M and Pilatus800k (Dectris) positioned at 2 m and 259 mm from the sample, respectively, were used to simultaneously collect small- and wide-angle X-ray scattering profiles. The total q-range was 0.09−30 nm^{-1}, with 30 s exposure for each measurement. A custom-made thermal stage was used to heat the samples to 60, 90, and 120 ˚C,

after which the samples were allowed to cool back to room temperature. Duplicate measurements were taken at the previously listed temperatures as the samples cooled. The SciAnalysis program (https://github.com/CFN-softbio/SciAnalysis) was used to perform the isotropic scattering data reduction into 1D patterns for further analysis.

Pulsed-Field-Gradient NMR Diffusometry and Spin Relaxation Measurements

Samples for ^{7}Li self-diffusion and spin-lattice (longitudinal) relaxation measurements were prepared by adding concentrated polymer solutions in methanol to 5 mm NMR tubes. Methanol was first evaporated at ambient temperature overnight and then removed in a vacuum oven at 30 °C for 72 h followed by another 72 h at 80 °C. The samples were cooled to room temperature under vacuum for another 72 h before flame sealing. ^{7}Li self-diffusion and spin-lattice relaxation measurements were performed on a Bruker Avance III 600 MHz spectrometer employing a Doty 5 mm, narrow bore (NB), Standard VT, ^{1}H-^{19}F/X PFG probe. The maximum Z-gradient available was 720 G/cm at 40 A current. NMR self-diffusion coefficients were measured using the pulsed-field-gradient stimulated echo (PGSTE) sequence with a longitudinal echo delay (LED) time of 20 ms and by varying (stepping) the gradient amplitude in 8–16 steps to generate successive spectra. As the gradient amplitude increases, the intensity of the echo signal (and spectral peak intensity) becomes attenuated by the translational diffusion of the molecules. The Stejskal-Tanner equation gives the signal attenuation, $I(g) = I(0)e^{-\gamma^2 g^2 \delta^2 \left(\Delta - \frac{\delta}{3}\right) D}$, where $I(0)$ is the echo intensity in the absence of any gradient, γ is the gyromagnetic ratio (1654.7 Hz/G for ^{7}Li), g is the gradient amplitude, δ is the effective duration time of the gradient pulse, Δ is the diffusion time, and D is

the diffusion coefficient. Sinusoidal gradient pulses of duration 4–7 ms and diffusion time, Δ of 100−800 ms were employed with the maximum gradient strength varying from 290 to 720 gauss/cm depending on the sample and temperature. Longitudinal spin relaxation time (T_1) measurements were carried out by the inversion-recovery method in 8 steps. The recycle delay (d1) was set to approximately $5\times T_1$, and the first T_1 delay time was set to 0.1 ms and the last T_1 delay time was set to approximately $5\times T_1$. Values of ^{7}Li T_1 at 80 °C and 150 °C are listed in **Table S3**.

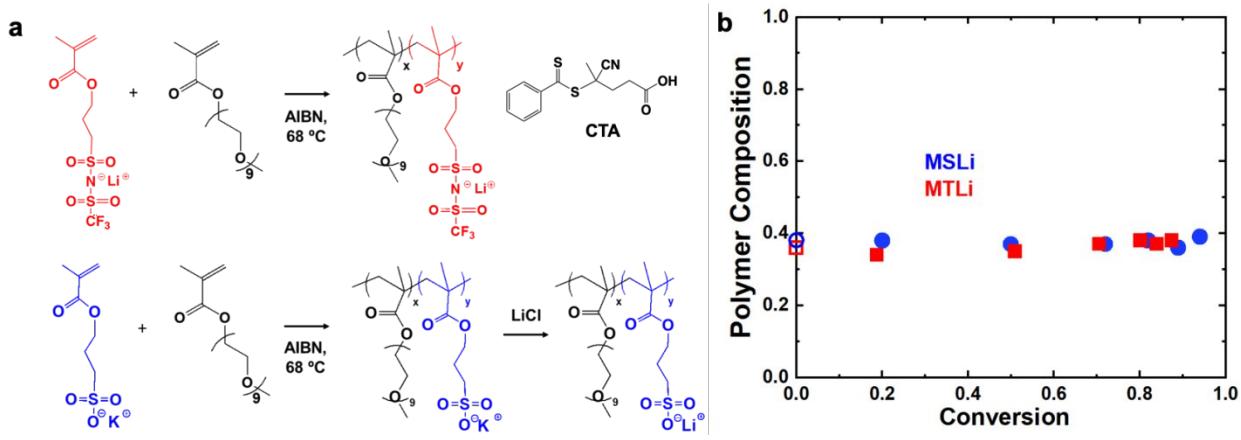

Figure 1. Synthesis of poly(ethylene oxide)-based sulfonylimide lithium (MTLi) and sulfonate lithium ionomers (MSLi). (a) The synthesis scheme of the ionomer with sulfonylimide lithium (top) and sulfonate lithium (bottom). (b) Copolymer molar composition of ionic monomers followed by ^{1}H NMR under different molar conversions shows minimal composition drift during the polymerization and indicates the synthesized ionomers are random with estimated reactivity ratios of 0.81 for MSK and 0.80 for PEO9 for the MSLi ionomers and 1.1 for both MTLi and PEO9 for the MTLi ionomers (with data from **Figure S4**).

Results and Discussion

A series of Li-ion conducting random copolymers containing poly(ethylene glycol) methacrylate (PEO9) and either sulfonylimide (MTLi) or sulfonate (MSLi) anion monomer units were synthesized using reversible addition-fragmentation chain transfer (RAFT) polymerization (**Figure 1**), resulting in ionomers with controlled M_n, narrow dispersity ($Đ$), and variable ion content. Increasing ion content increases the measured DSC glass transition temperature (T_g) for random ionomers due to increased monomer friction.[51-53] The T_g ranges from 223 K to 270 K for MTLi (ion content between 0.2–0.52) and from 221 K to 234 K for MSLi (ion content between 0.19 to 0.5, see **Table 1 and Figure S5**). By copolymerizing two methacrylate monomers with proper chain transfer agent, the synthesized ionomers are random copolymers with minimal compositional drift during the progression of the polymerization as indicated in **Figure 1b**. Specifically, the synthesized copolymer exhibits similar monomer composition as that of the initial monomer feed at all conversions (**Figure 1b**). Furthermore, the final copolymer composition closely follows that of the monomer feed for all the investigated ionomers with a conversion of ~ 80 mol% (**Figure S4a**). Characterization results for the synthesized ionomers are listed in **Table 1**, and the relevant details are included in Supporting Information.

Figure 2 demonstrates much faster ion conduction and Li-ion diffusivities for MTLi than MSLi copolymers. The conductivity (σ_{DC}) of the synthesized MTLi and MSLi ionomers were measured from 243–423 K with dielectric relaxation spectroscopy (DRS) (**Figure 2a**). The Li^+ self-diffusion coefficients D_{Li+} were measured with PFG NMR diffusometry and the values at different temperatures are plotted in **Figure 2b**. Firstly, MTLi ionomers show more than an order of magnitude higher σ_{DC} than MSLi at elevated temperatures (e.g., 150 °C) irrespective of the T_g difference (**Table 1** and **Figure 2a**). Secondly, the σ_{DC} changes more significantly with ion content for MTLi than MSLi as a consequence of the larger T_g difference for the former (**Table 1**). While the σ_{DC} difference is more than two orders of magnitude between MTLi20 and MTLi52 below 333 K, the σ_{DC} difference is within an order of magnitude for MSLi19 and MSLi48 over the entire measured temperature range since their T_g values only differ by 11 K. The huge D_{Li+} difference compared with σ_{DC} between MTLi52 and MTLi20 at elevated temperatures is due to the slowing down of Li^+ motion via Li^+ exchanging between ion aggregates, which will be further discussed. σ_{DC} follows the trend of D_{Li+} (**Figure 2b**), with a surprisingly low D_{Li+} for MSLi19 due to significant ion aggregation which will be further discussed. D_{Li+} is not measurable below 433 K for MSLi37 and MSLi48.

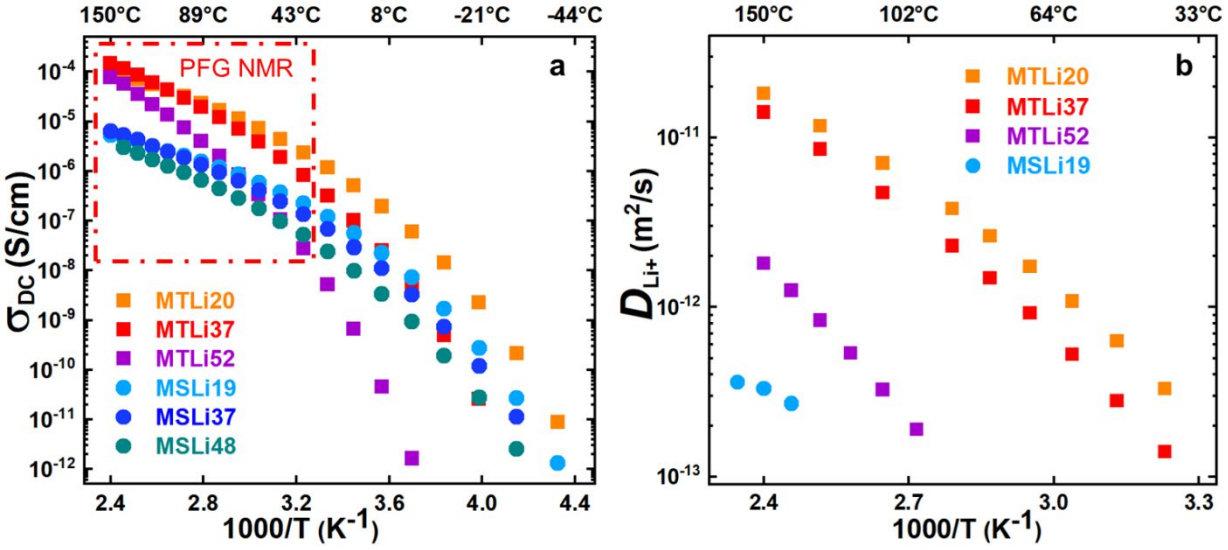

Figure 2. Conductivity and Li^+ diffusion for MSLi and MTLi ionomers as a function of temperature. (a) Temperature dependence of ionic conductivity σ_{DC} from DRS and (b) Li^+ self-diffusion coefficient D_{Li+} from NMR. MSLi19 can only be measured at ≥ 140 ˚C, and D_{Li+} for MSLi37 and MSLi48 cannot be measured (due to rapid NMR signal decay) from 313 to 433 K.

X-ray scattering measurements show that the formation of ion aggregates underlies the differences in σ_{DC} and D_{Li+} for MTLi and MSLi, which is supported from X-ray scattering measurements (**Figure 3**). **Figure 3a** shows the combined SAXS and WAXS data at 393 K plotted on logarithmic scales. The patterns have been vertically shifted to overlap scattering data from two different detectors (SAXS and WAXS) and cover the full q-range. The X-ray patterns clearly show three main peaks for all ionomers, located at $q \approx 14$ nm^{-1}, $q \approx 9$ nm^{-1}, and at low q (1−3 nm^{-1}) (1.8 nm^{-1}

for MSLi and 2.5 nm^{-1} for MTLi). The combined X-ray patterns were also vertically shifted on the log intensity scale to superimpose the high-q peaks located at 14 nm^{-1}, which is consistent for all the ionomers and corresponds to the amorphous halo (dominated by PEO9 side groups and pendent-to-pendant spacing).[54, 55] The second high-q peak (q_{anion} **Figure 3a**) at 9 nm^{-1} is attributed to the correlation between neighboring ion pairs solvated in the PEO matrix and from the anions due to the large electron density of S.[56] The corresponding correlation length d_{anion} ($d_{anion} = 2\pi/q_{anion}$) is 0.7 nm for MTLi and 0.8 nm for MSLi. The low-q peak ($q_{aggregate}$, **Figure 3a**) is attributed to the correlation between ion aggregates, with a correlation length $d_{aggregate}$ of 3.5–4.4 nm for MSLi and 2.5 nm for MTLi. The 3.5−4.4 nm spacing between ion aggregates for MSLi is typical for ionomers,[57] while 2.5 nm for MTLi is unusual, and suggests ion aggregates are far smaller and closer together.

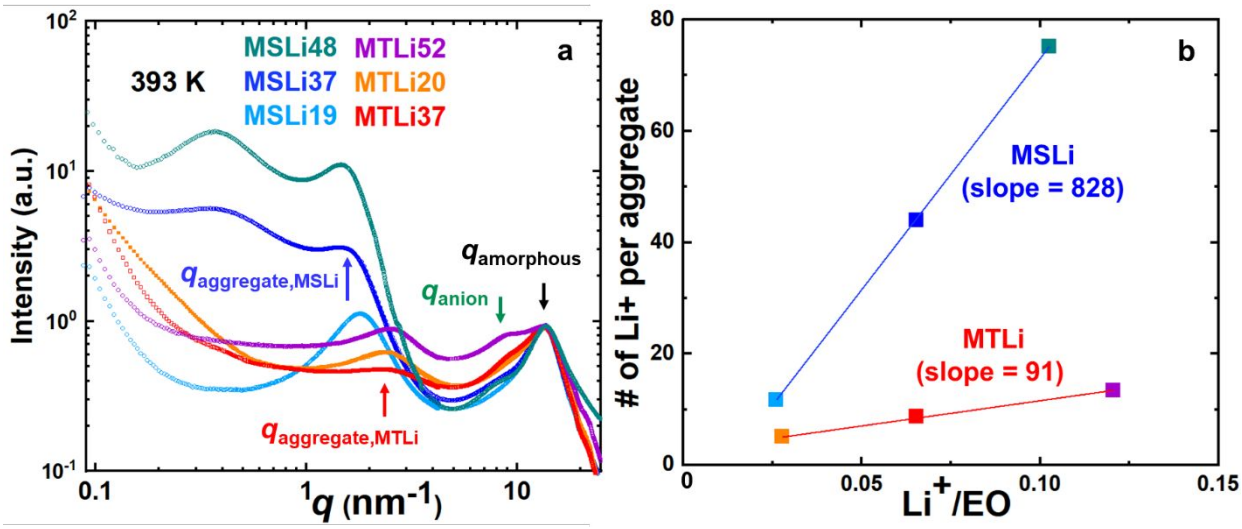

Figure 3. Combined SAXS and WAXS analysis of MSLi and MTLi ionomers as a function of ion content. (a) Scattering plots at 393 K, with intensities normalized to the peak at 14 nm^{-1} and peak assignments indicated with arrows. (b) Estimated Li^+ aggregation number (Eq. 1) plotted against Li^+/EO molar ratio. Higher ion contents include more ions in the aggregates and the sulfonated ionomers exhibit drastically more ion aggregation than the sulfonylimide-based ionomers. The considerably larger slope of MSLi than MTLi indicates a stronger aggregation tendency for the sulfonate-based system.

The X-ray scattering plots shown in **Figure 3a** indicate that MSLi ionomers form larger sulfonate lithium-ion aggregates with longer inter-aggregate spacing, as indicated from the high relative intensity and lower q value, respectively, compared to the MTLi ionomers (see blue and red arrows). For MSLi with increasing ion content, the relative intensity for the ionomer peak located

around $q = 1.8$ nm^{-1} increases considerably and shifts to lower q. The increase in intensity suggests more severe ion aggregation for MSLi with increasing ion content. Furthermore, the increased aggregation of ion pairs in MSLi ionomers results in fewer solvated Li^+ ions in the PEO matrix, resulting in a weak anion-anion correlation peak at 9 nm^{-1}. Interestingly, MSLi37 and MSLi48 exhibit a pronounced low-q scattering peak at $q = 0.4$ nm^{-1}. Although the exact cause of the peak is still currently under investigation, the peak is predicted to arise from either the shape of the aggregates or larger length scale heterogeneity. Previously published experimental works have seen similar low-q scattering features and simulations suggest that larger length scale heterogeneity is possible.[58-67]

In contrast to MSLi, in MTLi the sulfonylimide-Li^+ pairs show substantially weaker ion aggregation, which is evident from the lower relative intensity and smaller corresponding spacing for the ionomer peak at $q = 2.5$ nm^{-1}. The relative intensity of the anion-anion correlation peak (see q_{anion} in **Figure 3a**) at $q = 9.0$ nm^{-1} increases with ion content for MTLi, indicating a larger number density of solvated ion pairs in the PEO matrix. Raising ion content drives ion aggregation, evident from the significantly higher relative intensity of the low-q ion aggregation peak for MTLi52. The

lower relative intensity of the ionomer peak for MTLi37 than MTLi20 is likely due to the reduced contrast between the ion aggregates and the ions solvated in the PEO matrix, because the higher number density of solvated ions in MTLi37 decreases the contrast between the ion aggregates and the PEO matrix. This effect will be further discussed below along with conductivity and Li^+ diffusion results.

To qualitatively compare the extent of ion aggregation for the investigated ionomers, the average number of ions per aggregate is derived assuming all the Li^+ are contained in aggregates with an average spacing $d_{aggregate} = 2\pi/q_{aggregate}$ identified from X-ray:[68]

$$\#\ of\ Li\ per\ aggregate = d_{aggregate}^3 n_0 \qquad \text{Eq.1}$$

where n_0 is the stoichiometric number density of Li^+ (**Table 1**). These results are shown in **Figure 3b,** demonstrating the severe ion aggregation of MSLi. Specifically, MSLi19 has more than 20 Li^+ per aggregate, and the aggregation number increases significantly for MSLi37 and MSLi48. In contrast, the aggregation number is less than 20 for all investigated MTLi ionomers. Strikingly, MSLi19 and MTLi52 show similar aggregation numbers despite the notable change in ion content (**Table 1**), highlighting the role of anion chemical composition on ionomer morphology. DFT

calculations support the strongly aggregated morphology with sulfonate-Li^+ pairs due to their larger binding energy (ΔE_{pair}) and a more stable quadrupole conformation (higher ΔE_{quad}) compared with sulfonylimide-Li^+ pairs.[69] The quadrupole factor $\Delta E_{quad}/2\Delta E_{pair}$ is 1.14 for sulfonylimide-lithium ion pair and 1.23 for sulfonate-lithium ion pair, indicating ion aggregation is more energetically favorable for the polymers with sulfonate anion. The X-ray results in **Figure 3a** are consistent with the DFT calculations. Details for DFT calculation and relevant discussions are in the Supporting Information.

To further support the effect of anion chemical composition on ion conduction and material morphology, permittivity spectra were measured using DRS (**Figure 4**). As seen in **Figure 4**, MSLi demonstrates a much weaker dielectric response than that of MTLi, presumably due to the presence of ion aggregates that are dielectrically less active (i.e., ion-pair dipoles are canceled via forming quadrupoles and/or very slow motion that is not measurable within the frequency range). **Figure 4** shows the real permittivity spectra for MSLi (**Figure 4a**) and MTLi (**Figure 4b**) at 393 K where dielectric constants ε_s are determined and compared. The ε_s is determined before the onset of electrode polarization (where the ε' shows a power-law dependence over ω) and the fits are

indicated with colored lines (see Eq. S2 and Eq. S3 for fitting equations and **Table S2** for fitting parameters). The ε_s increases from 29 to 132 with ion content for MTLi. In contrast, the ε_s does not vary for MSLi and has a small value (≈ 10). The DRS measurements show excellent consistency with the interpreted morphology based on the X-ray results (**Figure 3**), where the number density of the solvated sulfonylimide-Li^+ pairs greatly outnumber that of the sulfonate-Li^+ pairs and raising copolymer ion content results in increased number density of the solvated ion pair for MTLi but not for MSLi. Consequently, MTLi show high ε_s due to the rotational motion of the ion pair dipole and the translational Li^+ diffusion, while the significantly aggregated sulfonate lithium-ion pairs barely respond to the applied electrical field, leading to the low ε_s of MSLi that is similar to the ε_s of the PEO side chains. The dielectric spectra results align with the morphology interpretation from X-ray and the D_{Li+} measured with NMR diffusometry (see below), indicating that ion aggregation, as driven by the anion chemistry, has a major impact on the ion mobility in ionomer materials like MSLi.

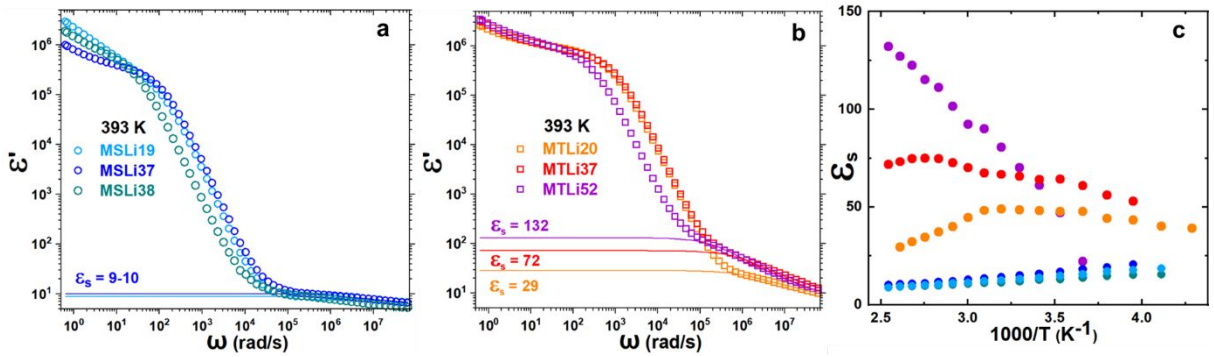

Figure 4. Angular frequency dependence of dielectric constant for MTLi and MSLi ionomers measured with DRS. Real permittivity spectra at 393 K for (a) MSLi and (b) MTLi. Lines represent the spectral fitting to determine the static dielectric constant ε_s. (c) Temperature dependence of ε_s for MTLi and MSLi.

Consistent with the general picture here, MSLi ionomers exhibit lower T_g and have significantly reduced molar conductivity Λ_{DC} with respect to T_g/T, as compared to MTLi ionomers (**Figure 5**). **Figure 5a** compares the measured DSC T_g for MTLi and MSLi ionomers and previously published ionomer work with respect to Li^+/EO molar ratio.[42, 70, 71] Data from this study are represented with filled symbols and data from the literature are shown with open symbols. The measured T_g for MTLi follows the T_g for the structurally similar ionomer poly(MTLi-*b*-PEO9) and poly(MTLi-*r*-PEO9),[70] while MSLi show much lower T_g than their PEO-based styrenic sulfonate lithium ionomer counterparts (PEO9-100Li, PEO13-100Li, and PEO24-100Li (See **Figure S10** for

structures).[42] The enhanced solvation of the sulfonylimide-Li^+ pair in PEO matrices results in higher T_g with increasing ion content (e.g., a 45 K T_g difference between MTLi20 with Li^+/EO = 0.028 and MTLi52 with Li^+/EO = 0.17). The poor solvation of sulfonate-Li^+ pairs due to their strong tendency for aggregation results in low T_g of the PEO-rich phase. The T_g corresponding to the ion aggregate phase is not accessible with DSC due to the high T_g value, masked by PEO degradation at elevated temperatures.[54, 72] The more significant ion aggregation for MSLi as compared to the PEO-100Li ionomers is likely due to the easier aggregation of ion pairs in MSLi enabled by the more flexible propyl methacrylate and the pendant ion placement as compared to the rigid styrene and the backbone ion placement in PEO-100Li.[73-75]

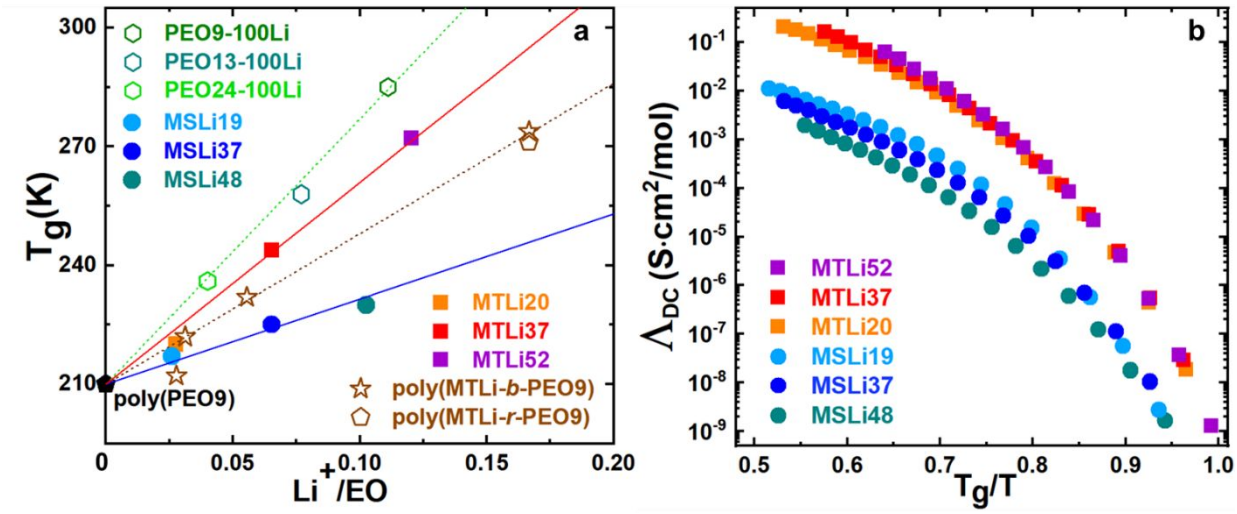

Figure 5. Effect of polymer chemical composition on T_g and ion conduction. (a) T_g of ionomers with sulfonylimide-lithium (MTLi, poly(MTLi-*b*-PEO9) and poly(MTLi-*r*-PEO9)) and sulfonate-lithium (MSLi, PEO9-100Li, PEO13-100Li and PEO24-Li) ion pairs with respect to Li^+/EO molar ratio. Filled symbols represent the ionomers studied here, and open symbols represent data from the literature.[42, 70, 71] (b) The molar conductivity Λ_{DC} compared at reduced temperature T_g/T is much lower for MSLi than MTLi due to severe ion aggregation (see **Figure 2**).

Figure 5b demonstrates an order of magnitude lower molar conductivity Λ_{DC} for MSLi than MTLi at the same reduced temperature T_g/T. Ion aggregation reduces the number density of charge carriers and their mobility drastically, which can explain the low Λ_{DC} of MSLi. Thus, although MSLi has reduced T_g (i.e., enhanced chain mobility), many of the Li ions are trapped in aggregates, reducing the number of available (non-neutralized) charge carriers.

Finally, the impact of ion aggregation on Li^+ conduction is further supported by ^{7}Li NMR diffusometry and spectroscopy measurements. First, note that mobile and immobile Li^+ are in dynamic exchange in the NMR timescale, as separate peaks are not observed for the mobile and immobile Li^+. The exchange between mobile and immobile Li^+ lowers the overall measured D_{Li+} for each sample, but by widely varying amounts depending on sample chemistry, ion concentration,

and resulting ion aggregate properties. **Figure 6a** compares the Haven ratio H for MTLi and MSLi (filled symbols) with literature data for PEO-100Li (open symbols). H is defined as the ratio of the NMR-derived conductivity σ_{NMR} and the DRS conductivity σ_{DC}. σ_{NMR} is derived from the $D_{\mathrm{Li+}}$ measured with NMR diffusometry (**Figure 2a**) and the stoichiometric ion number density n_0 (**Table 1**) based on the Nernst-Einstein equation ($\sigma_{NE} = \frac{n_0 e^2 D_{Li+}}{k_B T}$), which assumes all ions move independently. H is expressed as:

$$H = \frac{\sigma_{NMR}}{\sigma_{DC}} = \frac{n_0 e^2 D_{Li+}}{k_B T \sigma_{DC}} \quad \text{Eq. 2}$$

For MTLi, $H < 10$, with H falling between 2–4 for MTLi20 and 2–10 for MTLi37. The H value for MTLi is similar to the literature value reported for block copolymers containing a sulfonylimide-lithium ionic block ($H \sim 4$–7) and is consistent with the similar T_g for PEO-based sulfonylimide-lithium ionomers shown in **Figure 5**.[34] Because the measured $D_{\mathrm{Li+}}$ represents the average ion diffusion, the fact that $H > 1$ for MTLi20 and MTLi37 indicates the presence of ion pairs can move by segmental motion and contribute to $D_{\mathrm{Li+}}$ but not to σ_{DC}.[42, 76-78] However, the relatively low T_g values for MTLi20 and MTLi37 along with their high conductivity and $D_{\mathrm{Li+}}$ and their relatively low H values reflect that the ion aggregates for these materials are substantially weaker and smaller than for the MSLi and PEO-styrenic systems. For MTLi52, ion aggregates are

stronger and larger as compared to MTLi20 and MTLi37. Surprisingly, $H \approx 1$ for MTLi52. A Haven ratio of one indicates that it is unlikely that the anion and Li^+ pair diffuse over ~ 1 nm.

Since the conductivity and D_{Li+} are so much lower for MSLi19, the T_g is lower compared to the MTLi system, and the ion aggregation number is larger. It is clear that the anion chemistry is playing a significant role in the aggregates in MSLi being both larger and stronger. For MSLi19, H is also ≈ 1, indicating that Li^+ motion is almost independent of anion motion. The slow Li^+ diffusion in MSLi19 and the phthalate PEO-100Li reflects the large spacing between ion aggregates (and the very dilute mobile/solvated Li^+ species), and thus the large energy barrier for Li^+ jumps between aggregates. Thus, D_{Li+} is only measurable at elevated temperatures ($T > 413$ K), reaching values two orders of magnitude slower than MTLi20, and near the lower limit of NMR measurements (~ 10^{-14} m^2/s), further substantiating the chemically specific detrimental role of ion aggregation on ion conduction.

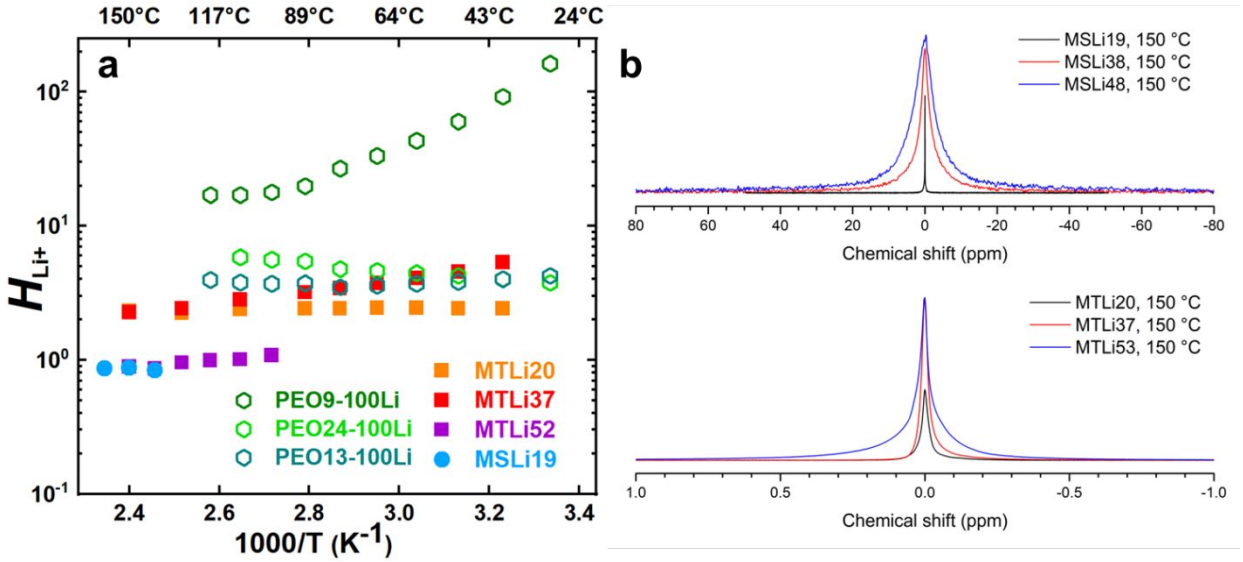

Figure 6. Temperature dependence of the Haven ratio (*H*) with respect to temperature and 1D ^{7}Li NMR spectra for synthesized and previously published ionomers. (a) *H* at different temperatures for ionomers MTLi and MSLi (filled symbols). Data for PEO-styrenic-based sulfonated lithium ionomers (open symbols) PEO9-100Li, PEO24-Li, and PEO13-Li are included for comparison.[25] (b) 1D ^{7}Li NMR spectra for MTLi and MSLi at 150 ˚C. Note the quite different ppm scales, where MTLi spectra show linewidths are far narrower than MSLi linewidths. The radio frequency (RF) pulse length was set to 5 μs for MSLi38 and MSLi48 to excite the full linewidth, and a 90˚ pulse length (19 μs) was used for all other samples.

1D ^{7}Li NMR spectra support the strongly aggregated morphology for MSLi and complement the understanding of the aggregated morphology on Li^+ conduction. **Figure 6b** compares the 1D ^{7}Li NMR spectra for MTLi and MSLi at 150 ˚C where MSLi shows considerably broader ^{7}Li NMR linewidths than MTLi (5−40 ppm vs. < 0.6 ppm). The broadening of the ^{7}Li NMR peak is due to

slow motions of the Li^+ local environment, most likely driven by strong ion aggregation evident in MSLi.[42, 45, 46, 79-81] Additionally, both MSLi and MTLi show broader ^7Li NMR linewidths with increasing ion content at a given temperature, due to slower motions and increased structural heterogeneity as aggregates grow in size and strength, which also results in broadening of the T_g range from DSC measurements (**Figure S5**).[54, 82]

These complementary characterization techniques – DSC, DRS, X-ray, NMR spectroscopy and diffusometry – pinpoint that anion chemical composition critically affects ion aggregation in ionomers and consequently ion conduction properties. The detrimental impacts of strong ion aggregation on Li^+ conduction is evident from MSLi where the traditional effort toward reducing T_g (i.e., reducing ion content and/or copolymerizing low T_g segments) is inadequate. In contrast, the sulfonylimide-lithium ionomers have a more delocalized anion and show smaller and weaker aggregates and raising the ion content brings the beneficial results of increased ion number density, though the D_{Li+} is reduced due to more substantial monomer friction.[51-53] Overall, this study emphasizes the critical role of ion aggregation on Li^+ conduction for ionomers and highlights the

necessity of breaking up ion aggregates via a proper choice of ion chemical composition to further promote ion transport for polymeric materials.

Conclusion

Six PEO-based Li-ion single-ion conducting ionomers with two types of anion structures, sulfonylimide (MTLi) and sulfonate (MSLi), were synthesized and characterized with DSC, DRS, X-ray scattering, and NMR. Severe ion aggregation in MSLi results in lower T_g, D_{Li+}, $\varepsilon_{s,}$ and σ_{DC}. In contrast, incorporating charge delocalized sulfonylimide anion leads to a less aggregated morphology with many tiny aggregates, raising $T_{g,}$ D_{Li+}, $\varepsilon_{s,}$ and σ_{DC} (see the summary in **Table 2**). Bulky, charge delocalized anions demonstrate alleviated aggregation morphology since the energetic gain for aggregation is less substantial compared with small, charged localized anions. The path forward would be synergizing bulky, charge-delocalized ions and low T_g, ion-solvating segments to achieve highly conductive single-ion conducting polymers.

Table 2. Summary of DSC, DRS, X-ray, and NMR results for MSLi and MTLi ionomers.

	MSLi	MTLi

DSC	lower T_g	higher T_g
	few ions in PEO	Many ions in PEO
DRS	lower ε_s	higher ε_s
	lower σ_{DC}	higher σ_{DC}
X-ray	more aggregation	less aggregation
	larger aggregates	many tiny aggregates
NMR	lower D_{Li+}	higher D_{Li+}
	broader ^{7}Li linewidth	sharper ^{7}Li linewidth

ASSOCIATED CONTENT

Supporting Information includes: I. Characterization of Single-ion Conductors with SEC and ^{1}H NMR; II. Glass Transition Temperature Characterized from Differential Scanning Calorimetry (DSC) and Dielectric Relaxation Spectroscopy (DRS); III. ^{7}Li NMR Measurements; IV. Comparing Sulfonate Anion and Sulfonylimide Anion Based on DFT Calculations.

The Supporting Information is available free of charge *via* the Internet.

AUTHOR INFORMATION

Corresponding Author

*E-mail: rhc5@psu.edu and rjh64@psu.edu

ORCID

Wenwen Mei:0000-0001-9777-3154

Deyang Yu: 0000-0003-0587-1211

Louis A. Madsen: 0000-0003-4588-5183

Ralph C. Colby: 0000-0002-5492-6189

Robert J. Hickey: 0000-0001-6808-7411

Notes

The authors declare no competing financial interest.

ACKNOWLEDGMENTS

We thank the National Science Foundation (NSF) for supporting this research through DMR 1807934. We thank Masafumi Fukuto and Ruipeng Li from Brookhaven National Lab for their help with X-ray measurements. The 11-BM CMS beamline of the National Synchrotron Light Source II was used, which is a US Department of Energy (DOE) Office of Science User Facility operated for the DOE Office of Science by Brookhaven National Laboratory under proposal number of 306118. We also thank Thomas Neuberger, Tapas Mal, Nicholas F. Pietra, and Shivam Gandhi for helping with the PFG NMR measurements.

References

1. Y. Zheng, Z. Yu, S. Zhang, X. Kong, W. Michaels, W. Wang, G. Chen, D. Liu, J.-C. Lai, N. Prine, W. Zhang, S. Nikzad, C. B. Cooper, D. Zhong, J. Mun, Z. Zhang, J. Kang, J. B. H. Tok, I. McCulloch, J. Qin, X. Gu and Z. Bao, *Nat. Commun.*, 2021, **12**, 5701.
2. M. L. Hammock, A. Chortos, B. C.-K. Tee, J. B.-H. Tok and Z. Bao, *Adv. Mater.*, 2013, **25**, 5997-6038.
3. S. J. Benight, C. Wang, J. B. H. Tok and Z. Bao, *Prog. Polym. Sci.*, 2013, **38**, 1961-1977.
4. M. Kaltenbrunner, T. Sekitani, J. Reeder, T. Yokota, K. Kuribara, T. Tokuhara, M. Drack, R. Schwödiauer, I. Graz, S. Bauer-Gogonea, S. Bauer and T. Someya, *Nature*, 2013, **499**, 458-463.
5. G. Li, R. Zhu and Y. Yang, *Nat. Photonics*, 2012, **6**, 153-161.
6. G. Wang, F. S. Melkonyan, A. Facchetti and T. J. Marks, *Angew. Chem. Int. Ed.*, 2019, **58**, 4129-4142.
7. Y.-J. Cheng, S.-H. Yang and C.-S. Hsu, *Chem. Rev.*, 2009, **109**, 5868-5923.
8. A. R. Murad, A. Iraqi, S. B. Aziz, S. N. Abdullah and M. A. Brza, *Polymers*, 2020, **12**, 2627.
9. J. Lopez, D. G. Mackanic, Y. Cui and Z. Bao, *Nat. Rev. Mater.*, 2019, **4**, 312-330.
10. Q. Zhao, S. Stalin, C.-Z. Zhao and L. A. Archer, *Nat. Rev. Mater.*, 2020, **5**, 229-252.
11. J. Li, Y. Cai, H. Wu, Z. Yu, X. Yan, Q. Zhang, T. Z. Gao, K. Liu, X. Jia and Z. Bao, *Adv. Energy Mater.*, 2021, **11**, 2003239.
12. D. Zhou, D. Shanmukaraj, A. Tkacheva, M. Armand and G. Wang, *Chem*, 2019, **5**, 2326-2352.
13. J. Liu, Z. Bao, Y. Cui, E. J. Dufek, J. B. Goodenough, P. Khalifah, Q. Li, B. Y. Liaw, P. Liu, A. Manthiram, Y. S. Meng, V. R. Subramanian, M. F. Toney, V. V. Viswanathan, M. S. Whittingham, J. Xiao, W. Xu, J. Yang, X.-Q. Yang and J.-G. Zhang, *Nat. Energy*, 2019, **4**, 180-186.
14. G. C. Righini, J. Krzak, A. Lukowiak, G. Macrelli, S. Varas and M. Ferrari, *Opt. Mater.*, 2021, **115**, 111011.
15. L. Trahey, F. R. Brushett, N. P. Balsara, G. Ceder, L. Cheng, Y.-M. Chiang, N. T. Hahn, B. J. Ingram, S. D. Minteer, J. S. Moore, K. T. Mueller, L. F. Nazar, K. A. Persson, D. J. Siegel, K. Xu, K. R. Zavadil, V. Srinivasan and G. W. Crabtree, *Proc. Natl. Acad. Sci.*, 2020, **117**, 12550-12557.
16. H. Zhang, C. Li, M. Piszcz, E. Coya, T. Rojo, L. M. Rodriguez-Martinez, M. Armand and Z. Zhou, *Chem. Soc. Rev.*, 2017, **46**, 797.
17. P. Albertus, V. Anandan, C. Ban, N. Balsara, I. Belharouak, J. Buettner-Garrett, Z. Chen, C. Daniel, M. Doeff, N. J. Dudney, B. Dunn, S. J. Harris, S. Herle, E. Herbert, S. Kalnaus, J. A. Libera, D. Lu, S. Martin, B. D. McCloskey, M. T. McDowell, Y. S. Meng, J. Nanda, J. Sakamoto, E. C. Self, S. Tepavcevic, E. Wachsman, C. Wang, A. S. Westover, J. Xiao and T. Yersak, *ACS Energy Lett.*, 2021, DOI: 10.1021/acsenergylett.1c00445, 1399-1404.
18. D. T. H. Jr. and N. P. Balsara, *Annu. Rev. Mater. Res.*, 2013, **43**, 503-525.
19. C. Y. Son and Z.-G. Wang, *J. Chem. Phys.*, 2020, **153**, 100903.
20. B. Boz, T. Dev, A. Salvadori and J. L. Schaefer, *J. Electrochem. Soc.*, 2021, **168**, 090501.
21. V. Bocharova and A. P. Sokolov, *Macromolecules*, 2020, DOI: 10.1021/acs.macromol.9b02742.
22. C. Cao, Y. Li, Y. Feng, C. Peng, Z. Li and W. Feng, *Energy Storage Mater.*, 2019, **19**, 401-407.

23. E. Strauss, S. Menkin and D. Golodnitsky, *J. Solid State Electrochem.*, 2017, **21**, 1879-1905.
24. M. Doyle, T. F. Fuller and J. Newman, *Electrochim. Acta*, 1994, **39**, 2073.
25. J. N. Chazalviel, *Phys. Rev. A*, 1990, **42**, 7355-7367.
26. J. L. Schaefer, Y. Lu, S. S. Moganty, P. Agarwal, N. Jayaprakash and L. A. Archer, *Applied Nanoscience*, 2012, **2**, 91-109.
27. R. Bouchet, S. Maria, R. Meziane, A. Aboulaich, L. Lienafa, J.-P. Bonnet, T. N. T. Phan, D. Bertin, D. Gigmes, D. Devaux, R. Denoyel and M. Armand, *Nat. Mater.*, 2013, **12**, 452-457.
28. E. W. Stacy, C. P. Gainaru, M. Gobet, Z. Wojnarowska, V. Bocharova, S. G. Greenbaum and A. P. Sokolov, *Macromolecules*, 2018, **51**, 8637.
29. D. Mecerreyes, *Prog. Polym. Sci.*, 2011, **36**, 1629-1648.
30. L. Meabe, N. Goujon, C. Li, M. Armand, M. Forsyth and D. Mecerreyes, *Batteries Supercaps*, 2020, **3**, 68-75.
31. J. F. Snyder, M. A. Ratner and D. F. Shriver, *J. Electrochem. Soc.*, 2003, **150**, A1090.
32. X.-G. Sun, J. B. Kerr, C. L. Reeder, G. Liu and Y. Han, *Macromolecules*, 2004, **37**, 5133-5135.
33. X.-G. Sun, C. L. Reeder and J. B. Kerr, *Macromolecules*, 2004, **37**, 2219-2227.
34. C. Jangu, A. M. Savage, Z. Zhang, A. R. Schultz, L. A. Madsen, F. L. Beyer and T. E. Long, *Macromolecules*, 2015, **48**, 4520-4528.
35. D. S.-d. la Cruz, M. D. Green, Y. Ye, Y. A. Elabd, T. E. Long and K. I. Winey, *J. Polym. Sci., Part B: Polym. Phys.*, 2012, **50**, 338-346.
36. Y. Ye and Y. A. Elabd, *Polymer*, 2011, **52**, 1309-1317.
37. R. L. Weber, Y. Ye, S. M. Banik, Y. A. Elabd, M. A. Hickner and M. K. Mahanthappa, *J. Polym. Sci., Part B: Polym. Phys.*, 2011, **49**, 1287-1296.
38. S. T. Hemp, M. Zhang, M. H. Allen Jr., S. Cheng, R. B. Moore and T. E. Long, *Macromol. Chem. Phys.*, 2013, **214**, 2099-2107.
39. H. Chen, J.-H. Choi, D. Salas-de la Cruz, K. I. Winey and Y. A. Elabd, *Macromolecules*, 2009, **42**, 4809-4816.
40. E. U. Mapesa, M. Chen, M. F. Heres, M. A. Harris, T. Kinsey, Y. Wang, T. E. Long, B. S. Lokitz and J. R. Sangoro, *Macromolecules*, 2019, **52**, 620-628.
41. U. H. Choi, Y. Ye, D. Salas de la Cruz, W. Liu, K. I. Winey, Y. A. Elabd, J. Runt and R. H. Colby, *Macromolecules*, 2014, **47**, 777.
42. N. H. LaFemina, Q. Chen, R. H. Colby and K. T. Mueller, *J. Chem. Phys.*, 2016, **145**, 114903.
43. U. H. Choi, M. Lee, S. Wang, W. Liu, K. I. Winey, H. W. Gibson and R. H. Colby, *Macromolecules*, 2012, **45**, 3974-3985.
44. S.-W. Wang, W. Liu and R. H. Colby, *Chem. Mater.*, 2011, **23**, 1862-1873.
45. M. Brinkkötter, E. I. Lozinskaya, D. O. Ponkratov, Y. Vygodskii, D. F. Schmidt, A. S. Shaplov and M. Schönhoff, *J. Phys. Chem. C*, 2019, **123**, 13225-13235.
46. M. Brinkkötter, E. I. Lozinskaya, D. O. Ponkratov, P. S. Vlasov, M. P. Rosenwinkel, I. A. Malyshkina, Y. Vygodskii, A. S. Shaplov and M. Schönhoff, *Electrochim. Acta*, 2017, **237**, 237-247.
47. D. P. Siska and D. F. Shriver, *Chem. Mater.*, 2001, **13**, 4698-4700.
48. S. Liang, U. H. Choi, W. Liu, J. Runt and R. H. Colby, *Chem. Mater.*, 2012, **24**, 2316-2323.

49. S. W. Liang, M. V. O'Reilly, U. H. Choi, H. S. Shiau, J. Bartels, Q. Chen, J. Runt, K. I. Winey and R. H. Colby, *Macromolecules*, 2014, **47**, 4428-4437.
50. C. Ren, M. Liu, J. Zhang, Q. Zhang, X. Zhan and F. Chen, *J. Appl. Polym. Sci.*, 2018, **135**, 45848.
51. K.-H. Shen, M. Fan and L. M. Hall, *Macromolecules*, 2021, **54**, 2031-2052.
52. K. I. S. Mongcopa, D. A. Gribble, W. S. Loo, M. Tyagi, S. A. Mullin and N. P. Balsara, *Macromolecules*, 2020, **53**, 2406-2411.
53. K. I. S. Mongcopa, M. Tyagi, J. P. Mailoa, G. Samsonidze, B. Kozinsky, S. A. Mullin, D. A. Gribble, H. Watanabe and N. P. Balsara, *ACS Macro Lett.*, 2018, **7**, 504-508.
54. J.-H. H. Wang, C. H.-C. Yang, H. Masser, H.-S. Shiau, M. V. O'Reilly, K. I. Winey, J. Runt, P. C. Painter and R. H. Colby, *Macromolecules*, 2015, **48**, 7273-7285.
55. W. Wang, W. Liu, G. J. Tudryn, R. H. Colby and K. I. Winey, *Macromolecules*, 2010, **43**, 4223-4229.
56. P. J. Brown, A. G. Fox, E. N. Maslen, M. A. O'Keefe and B. T. M. Willis, in *International Tables for Crystallography Volume C: Mathematical, physical and chemical tables*, ed. E. Prince, Springer Netherlands, Dordrecht, 2004, DOI: 10.1107/97809553602060000600, pp. 554-595.
57. K. M. Beers and N. P. Balsara, *ACS Macro Lett.*, 2012, **1**, 1155-1160.
58. R. A. Register, *Macromolecules*, 2020, **53**, 1523-1526.
59. C. E. Williams, T. P. Russell, R. Jerome and J. Horrion, *Macromolecules*, 1986, **19**, 2877.
60. D. J. Yarusso and S. L. Cooper, *Macromolecules*, 1983, **16**, 1871-1880.
61. A. Eisenberg and M. Navratil, *Macromolecules*, 1974, **7**, 90-94.
62. C. L. Marx, D. F. Caulfield and S. L. Cooper, *Macromolecules*, 1973, **6**, 344.
63. K. Lu, J. F. Rudzinski, W. G. Noid, S. T. Milner and J. K. Maranas, *Soft Matter*, 2014, **10**, 978-989.
64. K.-J. Lin and J. K. Maranas, *Macromolecules*, 2012, **45**, 6230-6240.
65. K. A. Page, F. A. Landis, A. K. Phillips and R. B. Moore, *Macromolecules*, 2006, **39**, 3939-3946.
66. J. A. Elliott, D. Wu, S. J. Paddison and R. B. Moore, *Soft Matter*, 2011, **7**, 6820-6827.
67. L. J. Abbott and J. W. Lawson, *Macromolecules*, 2019, **52**, 7456.
68. A. Mordvinkin, M. Suckow, F. Böhme, R. H. Colby, C. Creton and K. Saalwächter, *Macromolecules*, 2019, **52**, 4169-4184.
69. H.-S. Shiau, W. Liu, R. H. Colby and M. J. Janik, *J. Chem. Phys.*, 2013, **139**, 204905.
70. L. Porcarelli, A. S. Shaplov, M. Salsamendi, J. R. Nair, Y. S. Vygodskii, D. Mecerreyes and C. Gerbaldi, *ACS Appl. Mater. Interfaces*, 2016, **8**, 10350.
71. S. Dou, S. Zhang, R. J. Klein, J. Runt and R. H. Colby, *Chem. Mater.*, 2006, **18**, 4288-4295.
72. G. J. Tudryn, M. V. O'Reilly, S. Dou, D. R. King, K. I. Winey, J. Runt and R. H. Colby, *Macromolecules*, 2012, **45**, 3962-3973.
73. C. M. Evans, C. R. Bridges, G. E. Sanoja, J. Bartels and R. A. Segalman, *ACS Macro Lett.*, 2016, **5**, 925-930.
74. L. J. Fetters, D. J. Lohse and R. H. Colby, in *Physical Properties of Polymers Handbook*, ed. J. E. Mark, Springer New York, New York, NY, 2007, DOI: 10.1007/978-0-387-69002-5_25, pp. 447-454.
75. L. J. Abbott and J. W. Lawson, *Macromolecules*, 2019, **52**, 7456-7467.
76. N. H. LaFemina, Q. Chen, K. T. Mueller and R. H. Colby, *ACS Energy Lett.*, 2016, **1**, 1179.

77. K. D. Fong, J. Self, B. D. McCloskey and K. A. Persson, *Macromolecules*, 2021, **54**, 2575-2591.
78. N. M. Vargas-Barbosa and B. Roling, *ChemElectroChem*, 2020, **7**, 367-385.
79. D. J. Roach, S. Dou, R. H. Colby and K. T. Mueller, *J. Chem. Phys.*, 2012, **136**, 014510.
80. J. Adebahr, M. Forsyth, D. R. MacFarlane, P. Gavelin and P. Jacobsson, *Solid State Ionics*, 2002, **147**, 303-307.
81. P. E. Stallworth, S. G. Greenbaum, F. Croce, S. Slane and M. Salomon, *Electrochim. Acta*, 1995, **40**, 2137-2141.
82. Q. Chen, N. Bao, J.-H. H. Wang, T. Tunic, S. Liang and R. H. Colby, *Macromolecules*, 2015, **48**, 8240-8252.